International Journal of Microwave and Wireless Technologies, 2009, 1(4), 285–292.
doi:10.1017/S1759078709990390 Printed in the United Kingdom

An L-band SiGe HBT differential amplifier with frequency and rejection-level tunable, multiple stopband

MASAKI SHIRATA, TOSHIO SHINOHARA, MINORU SATO AND YASUSHI ITOH

An L-band frequency and rejection-level tunable SiGe HBT differential amplifier with dual stopband is presented. To achieve frequency and rejection-level tunable performance, dual LCR-tank circuit with an active load is incorporated into the design of the series feedback loops of the differential amplifier. The active load consists of a varactor diode represented as a variable C *and a common-emitter transistor represented as a variable* R*. The frequency and rejection level can be tuned independently by controlling a cathode bias voltage of the varactor diode or a base bias voltage of the transistor. The implemented 0.35 μm SiGe HBT amplifier with dual stopband demonstrates a frequency tuning of 0.53–1.16 GHz and a rejection-level variation up to 9.5 dB. The input and output return losses are better than 17.5 and 11 dB over 0.2–1.5 GHz, respectively. The measured P1dB is + 3 dBm and IIP3 is 0 dBm with* Vcc = *6 V and* Ic = *8 mA.*

Keywords: Differential amplifier, Tunable, Microwave, SiGe HBT, Bandstop, Multiple band

Received 13 January 2009; Revised 15 April 2009; first published online 22 June 2009

I. INTRODUCTION

With the rapid and increasing growth of wireless and mobile communication systems, the multi-band and multi-mode systems and applications for wide-area and local-area wireless systems are being actively researched and developed by many countries in the world [1], including WLAN 802.11a/b/g [2], GSM800MHz/GSM1.8GHz [3], and ISM2&5GHz [4]. For the multi-band and multi-mode applications, however, the interference and image rejection of collocated active radios in both frequency and space become a crucial issue [5]. To address this problem, the CMOS LNA with image rejection filters [6, 7] and the differential phase rotator [5] have been proposed as an active interference canceller. The CMOS LNA [6, 7] employs a stacked common-gate topology, thus not suitable for differential amplification. The canceller system using the differential phase rotator [5] is complex in circuit topology and provides an additional loss. In addition, these circuits have a difficulty to be applied to multi-band and multi-mode operation.

In order to address these problems, an SiGe HBT differential amplifier with frequency and rejection-level tunable, multiple stopband is devised mainly for WLAN 802.11 a/b/g applications. It employs a multiple LCR-tank circuit, which is cascaded in a stacked form and connected between emitters of the differential transistor pair to achieve multiple bandstop performance. Each LCR-tank circuit employs an active load comprised of a varactor diode represented as a variable *C* for frequency tuning and a common-base transistor represented as a variable *R* for rejection-level tuning.

Department of Electrical and Electronic Engineering, Shonan Institute of Technology, 1-1-25 Tsujido-Nishikaigan, Fujisawa, Kanagawa 251-8511 Japan. Phone & Fax: +81-466-30-0185.
Corresponding author:
Y. Itoh
Email: itohy@center.shonan-it.ac.jp

Basically the multi-band amplifiers are categorized into three basic groups. The first group achieves multi-band performance by switching amplifiers, matching circuits, or bias [8]. The second group employs a concurrent matching technique [9, 10]. The third group is a wideband amplifier [11]. The first group has a non-operating amplifier or matching circuits, leading to a large size and high power consumption. The circuit design of the second group is rather complicated, thus limiting the number of bands to dual band. The third group amplifies the unwanted signals at the same time. The stacked LCR-tank circuit presented in this paper has an advantage over the conventional groups in circuit size, circuit design simplicity, power consumption, suppression of the unwanted signals, and applicability of multiple bands [12].

As a frequency-tunable device, the varactor-tuned, frequency-agile microwave filter with bandpass or bandstop performance is widely used [13]. Since it is comprised of distributed microstrip or coplanar lines combined with varactor diodes, the circuit size becomes much larger in the multi-band and multi-mode applications. To overcome this problem, lumped LC elements are utilized in this amplifier in order to achieve a miniaturized size. Moreover, with the use of a stacked configuration, multiple bandstop frequencies can be tuned independently by adjusting a control voltage of the varactor diode.

The amplifier presented in this paper has made great advances over the previously reported ones [14, 15] in that only frequency was varied in ref. [15] but frequency, rejection-level, and number of rejection peaks can be varied with the introduction of active loads. Moreover, the design approaches and measured results on how to improve noise figure and IIP_3 are presented. The frequency and rejection-level tunable performance for multiple stopband are promising as an active interference canceller for the next-generation, adaptive and/or reconfigurable wireless radios.

II. CIRCUIT DESIGN

A schematic diagram of the frequency and rejection-level tunable differential amplifier with dual stopband is shown in Fig. 1. The amplifier employs a dual LCR-tank circuit with an active load in the design of the series feedback loops of the differential amplifier. The active load consists of a varactor diode as a variable C and a common-emitter transistor as a variable R. V_{c1} and V_{c2} are control voltage of the varactor diode and V_{c3} and V_{c4} are control voltage of the transistor. A low-frequency gain of the differential amplifier (G_L) is given as [16]

$$G_L = |Z_L Y_S|, \tag{1}$$

where Z_L is a load impedance consisting of an inductor L_o and a resistor R_o. Y_S is an admittance of the dual LCR-tank circuit. A simplified schematic diagram of Fig. 1 is shown in Fig. 2. An LCR-tank circuit is represented as a parallel connection of a fixed L, a variable C, and a variable R. With the use of the admittances of each LCR-tank circuit (Y_1 and Y_2) and the load impedance Z_L, a low-frequency gain G_L in Eq. (1) can be obtained as follows:

$$G_L = |Z_L| \bullet \left| \frac{Y_1 Y_2}{Y_1 + Y_2} \right| \tag{2}$$

$$|Z_L| = \sqrt{R_o^2 + (\omega L_o)^2} \tag{3}$$

$$|Y_1 Y_2| = \sqrt{\begin{bmatrix} \frac{1}{R_1^2} + \omega^2 C_1^2 \left\{ 1 - \left(\frac{\omega_{C1}}{\omega} \right)^2 \right\}^2 \end{bmatrix} \bullet \begin{bmatrix} \frac{1}{R_2^2} + \omega^2 C_2^2 \left\{ 1 - \left(\frac{\omega_{C2}}{\omega} \right)^2 \right\}^2 \end{bmatrix}} \tag{4}$$

$$|Y_1 + Y_2| = \sqrt{\left(\frac{1}{R_1} + \frac{1}{R_2} \right)^2 + \omega^2 (C_1 + C_2)^2 \left\{ 1 - \left(\frac{\omega_{C3}}{\omega} \right)^2 \right\}^2} \tag{5}$$

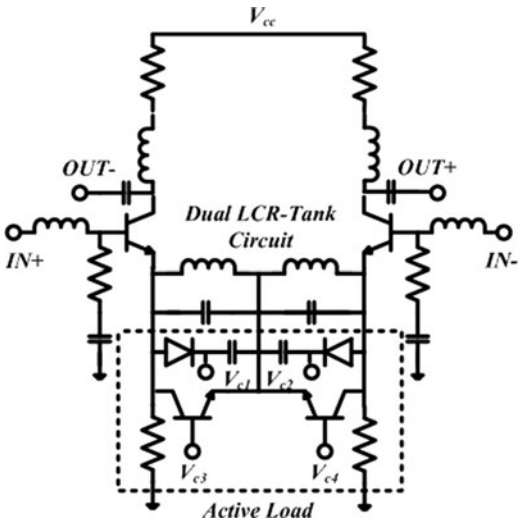

Fig. 1. Schematic diagram of the frequency and rejection-level tunable differential amplifier with dual stopband.

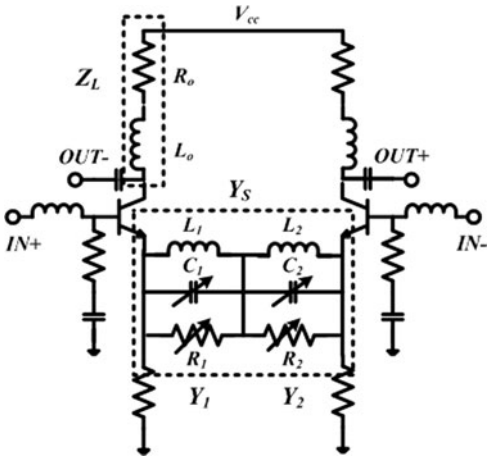

Fig. 2. Simplified schematic diagram of Fig. 1.

$$\omega_{C1} = \frac{1}{\sqrt{L_1 C_1}} \tag{6}$$

$$\omega_{C2} = \frac{1}{\sqrt{L_2 C_2}} \tag{7}$$

$$\omega_{C3} = \sqrt{\frac{1/L_1 + 1/L_2}{C_1 + C_2}} \tag{8}$$

It is noted in Eqs (2) to (8) that a low-frequency gain G_L has a single gain peak at ω_{C3} as well as double rejection peaks at ω_{C1} and ω_{C2}, which is roughly displayed in Fig. 3. If $\omega_{C1} < \omega_{C2}$, then ω_{C1}, ω_{C2}, and ω_{C3} necessarily satisfy the condition that $\omega_{C1} < \omega_{C3} < \omega_{C2}$. The frequency and rejection level can be tuned independently by controlling the value of C_1 (V_{c1}), C_2 (V_{c2}), R_1 (V_{c3}), or R_2 (V_{c4}). Cascading additional LCR-tank circuits in a stacked form can easily increase the number of rejection peaks.

A design example of the simulated gain and return loss of the amplifier is shown in Fig. 4, where V_{cc} is a supply voltage. The bias conditions are $V_{cc} = V_{c1} = V_{c2} = 6$ V and $V_{c3} = V_{c4} = 6.6$ V, respectively. The circuit simulation was accomplished for the schematic diagram shown in Fig. 1, where 0.35 μm SiGe HBTs (Toshiba MT4S102T) with $f_t = 25$ GHz and silicon varactor diodes (Toshiba 1SV279) with $C_{2V} = 15$ pF, $C_{10V} = 6$ pF are used. In Fig. 4, f_1 and f_2 are a stopband. Since an averaged gain of the amplifier without LCR-tank circuits is around 10 dB from 0.2 to 1.5 GHz, a rejection level of around 14 dB at f_1 and f_2 is accomplished. Input and output return losses are better than 12 dB at f_1 and f_2.

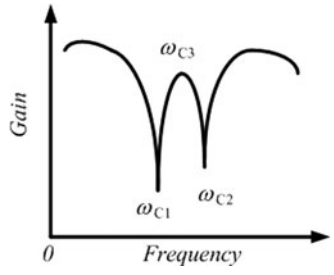

Fig. 3. Gain and rejection peaks of the amplifier.

https://doi.org/10.1017/S1759078709990390 Published online by Cambridge University Press

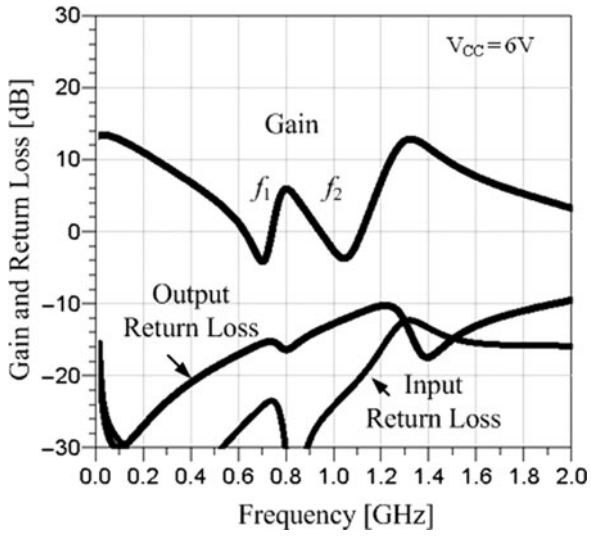

Fig. 4. Simulated gain and return loss of the frequency and rejection-level tunable differential amplifier with dual stopband.

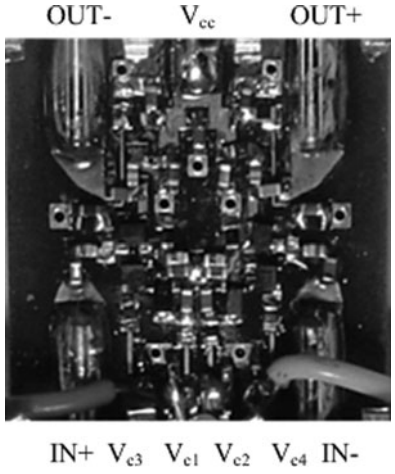

Fig. 5. Photograph of the frequency and rejection-level tunable differential amplifier with dual stopband.

III. CIRCUIT FABRICATION

A photograph of the frequency and rejection-level tunable differential amplifier with dual stopband is shown in Fig. 5. The amplifier was fabricated on the FR-4 substrate with a dielectric constant of 4.5. 1005-type chip inductors, capacitors, and resistors are mounted on the substrate by soldering. The circuit size is $16 \times 16 \times 1.2$ mm^3.

IV. CIRCUIT PERFORMANCE

A) Gain and return loss

The measured gain and return loss of the amplifier are shown in Fig. 6. The measurement was done on the condition that $V_{cc} = V_{c1} = V_{c2} = 6$ V and $V_{c3} = V_{c4} = 6.6$ V. The measured gain and return losses are in good agreement with the simulated ones in Fig. 4, showing a slight discrepancy for rejection level. As compared with the measured result of the amplifier that does not have a common-emitter transistor as a variable R [15], the overall gain drops by approximately 1 dB but the input and output return losses are almost the same.

B) Frequency tunable performance

As mentioned above, the bandstop frequencies (f_1 and f_2) can be tuned independently with the control of V_{c1} or V_{c2}. The measured results on the condition that f_1 is varied and f_2 is fixed are introduced first. Then the measured results on the condition that f_1 is fixed and f_2 is varied are demonstrated. The measured gain, input return loss, and output return loss are shown in Figs 7–9 on the condition that V_{c1} varies from 2 to 10 V for a fixed value of $V_{c2} = 10$ V.

It is shown in Fig. 7 that the bandstop frequency f_1 can be tuned from 0.5 to 0.8 GHz for a fixed value of $f_2 = 1.1$ GHz. The rejection-level changes from 11.2 to 15.5 dB for a variation of f_1. As shown in Figs 8 and 9, the input and output return losses are better than 25 and 15 dB, respectively, for a variation of f_1. The measurement was done at $V_{cc} = 6$ V and $V_{c3} = V_{c4} = 6.6$ V.

On the other hand, the measured gain, input return loss, and output return loss are demonstrated in Figs 10–12 on the condition that V_{c2} varies from 2 to 10 V for a fixed value of $V_{c1} = 2$ V. It is shown in Fig. 10 that the bandstop frequency f_2 can be tuned from 0.6 to 1.1 GHz for a fixed value of $f_1 = 0.6$ GHz. The rejection-level changes from 11.5 to 17.5 dB for a variation of f_2. As clearly shown in Figs 11 and 12, the input and output return losses are better than 17.5 and 11 dB, respectively, for a variation of f_2. The measurement was done at $V_{cc} = 6$ V and $V_{c3} = V_{c4} = 6.6$ V.

A stability factor for frequency tunable performance was calculated and plotted in Fig. 13. The calculated results are almost the same for both Figs 7 and 10. Thus only the calculated K-factor for Fig. 7 was shown in Fig. 13. As f_1 comes near to f_2, the K-factor decreases but becomes constant to around 1.2, showing an unconditionally stable condition.

C) Rejection-level tunable performance

The rejection level at a stopband can be tuned by varying the value of R_1 or R_2 in Fig. 2. A variable R_1 or R_2 is obtained from a differential value of the I–V curves of the transistor at $V_{CE} = 0$ V. A typical example of the I–V characteristics of the transistor is shown in Fig. 14. The solid and dotted lines

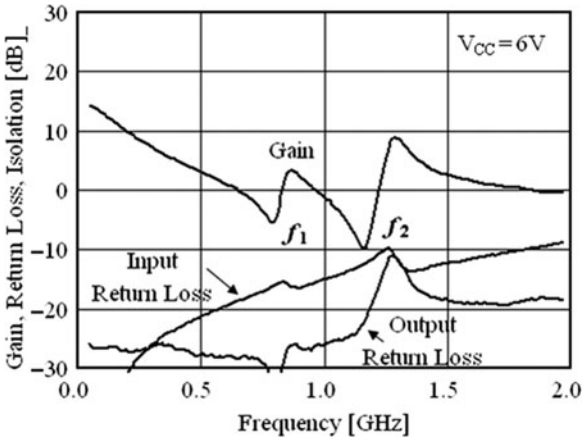

Fig. 6. Measured gain and return loss of the frequency-tunable, dual-stopband differential amplifier.

https://doi.org/10.1017/S1759078709990390 Published online by Cambridge University Press

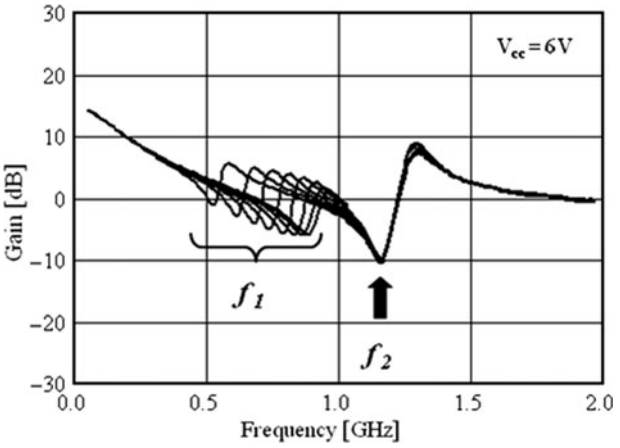

Fig. 7. Measured gain for a varied value of V_{c1} and a fixed value of V_{c2}.

show I–V curves and differential values at $V_{CE} = 0$, respectively. As clearly shown in Fig. 14, a differential value of the I–V curves varies with a parameter of I_B or V_B at $V_{CE} = 0$ V. Actually, a variable R_1 or R_2 is realized by using the output impedance of the transistor with a parameter of V_B for $V_{CE} = 0$ V.

The measured results on the condition that V_{c3} is varied from 6.6 to 7.4 V and V_{c4} is fixed to 6.6 V are shown in Fig. 15. Then the measured results on the condition that V_{c3} is fixed to 6.6 V and f_2 is varied from 6.6 to 7.4 V are displayed in Fig. 16. V_{cc}, V_{c1}, and V_{c2} are 6 V.

The rejection level varies from 1 to 6 dB at f_1 with the control of V_{c3}. On the other hand, the rejection level varies from 0.5 to 10 dB at f_2 with the control of V_{c4}. From these results, a rejection level up to 9.5 dB has been achieved across 0.53–1.16 GHz. No outstanding changes appeared for the input and output return losses. As similar to the frequency-tuning performance, the rejection level can be also varied independently.

In an actual application of the wireless systems, for example, the interference cancellation or image-rejection ratio of greater than 80 dB could be needed. The bandstop filters with 30 dB of band-rejection ratio are connected before and after the amplifier. Thus a band-rejection ratio of greater than 20 dB is required for the amplifier, which can be easily achieved by employing a multi-stage design.

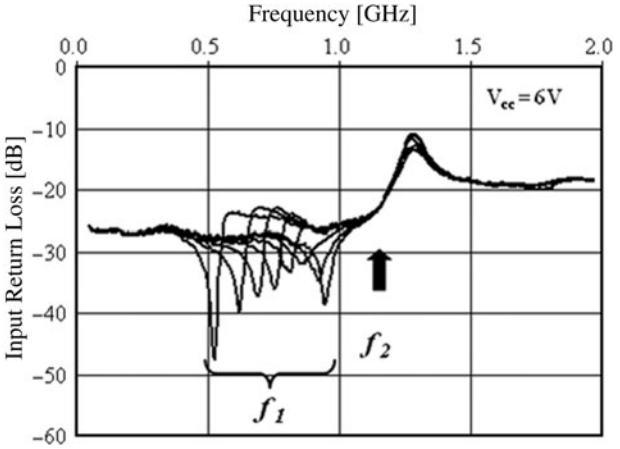

Fig. 8. Measured input return loss for a varied value of V_{c1} and a fixed value of V_{c2}.

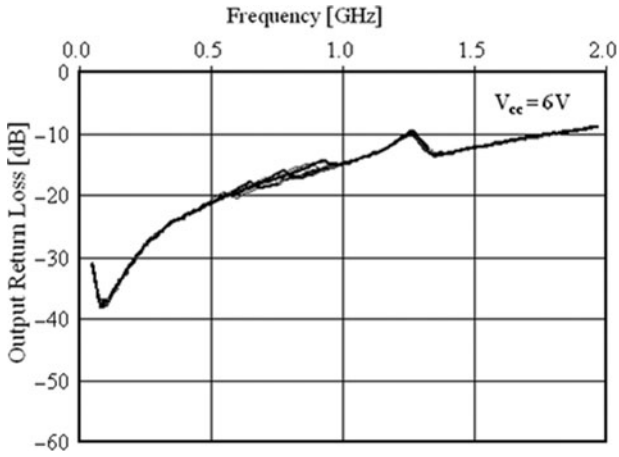

Fig. 9. Measured output return loss for a varied value of V_{c1} and a fixed value of V_{c2}.

D) Number of rejection peaks

As an application of the frequency-tunable performance, the number of rejection peaks (the number of stopband) can be varied. At a starting point, two bandstop frequencies (f_1 and f_2) are separated as far as possible. Then V_{c1} and V_{c2} are controlled so that two separate frequencies (f_1 and f_2) come near and finally become a single frequency (single band). The measured variation of the number of rejection peaks (the number of stopband) with the control of V_{c1} and V_{c2} is shown in Fig. 17. f_1 moves from 0.6 to 0.8 GHz for a variation of V_{c1} from 6 to 13 V. Inversely, f_2 moves from 1.2 to 0.8 GHz for a variation of V_{c2} from 13 to 6 V. In a similar way, a variation from single band to dual band is also possible.

E) Noise figure

The noise figure measurement was done for the pass-band region from 1.0 to 1.2 GHz with $f_1 = 0.8$ GHz and $f_2 = 1.1$ GHz. The measured results are shown in Fig. 18. The measured best noise figure was 5.6 dB at 1.1 GHz. The bias conditions were $V_{cc} = 6$ V and $I_c = 8$ mA. Considering the F_{min} of 0.4 dB at 1 GHz of the 0.35 μm SiGe HBT, the measured NF shows a poor performance because the amplifier employs a lossy match configuration to achieve a wide

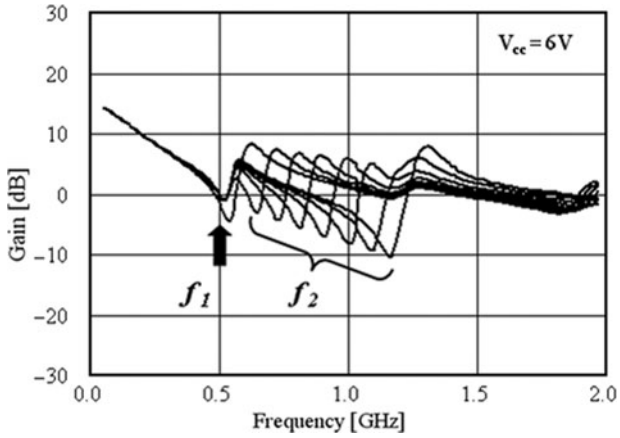

Fig. 10. Measured gain for a varied value of V_{c2} and a fixed value of V_{c1}.

https://doi.org/10.1017/S1759078709990390 Published online by Cambridge University Press

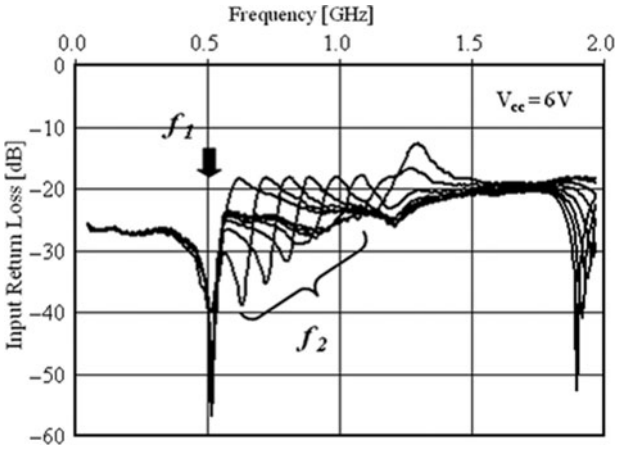

Fig. 11. Measured input return loss for a varied value of V_{c2} and a fixed value of V_{c1}.

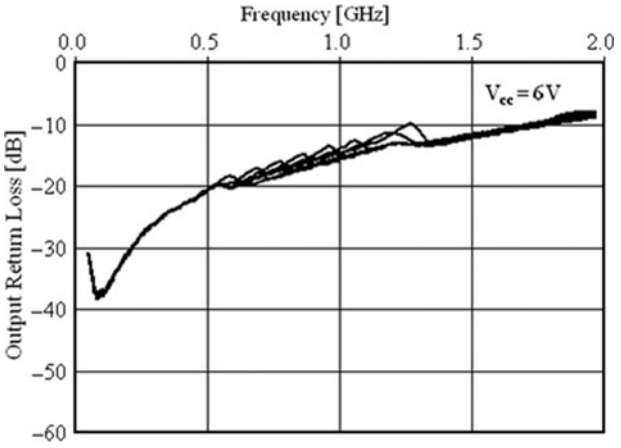

Fig. 12. Measured output return loss for a varied value of V_{c2} and a fixed value of V_{c1}.

bandwidth and high stability. The noise figure can be improved with the employment of reactive matching in place of lossy matching, sacrificing bandwidth. A schematic diagram of lossy match and reactive match configurations is shown in Fig. 19. The noise figure was measured for the reactive match configuration in Fig. 19 (b) and also plotted in Fig. 18. The measured best noise figure was 1.2 dB

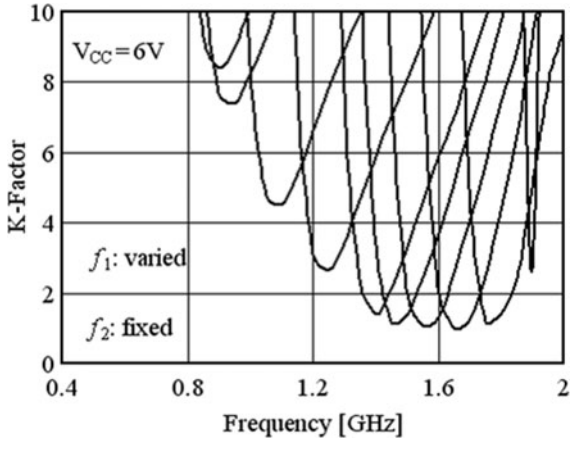

Fig. 13. Calculated *K*-factor for a varied value of f_1 and a fixed value of f_2.

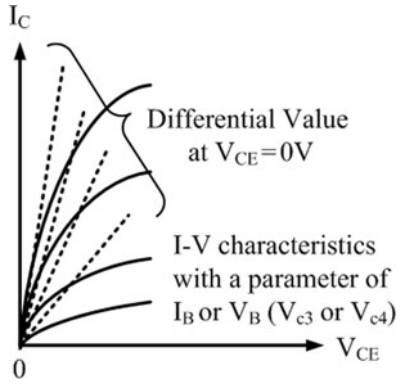

Fig. 14. *I–V* characteristics of the transistor.

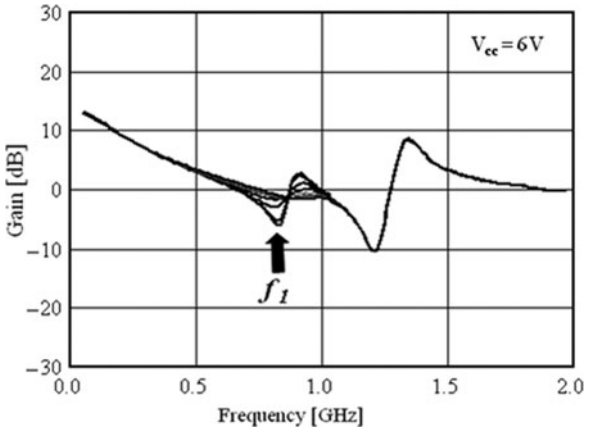

Fig. 15. Measured gain for a varied value of V_{c3} and a fixed value of V_{c4}.

at 1 GHz, showing a significant improvement of 4.4 dB. But the frequency tuning range becomes narrow from 0.53–1.16 GHz down to 0.8–1.2 GHz.

F) IIP3

In order to achieve a high dynamic range of the low-noise amplifier, a low noise figure along with a high IIP_3 is required. To achieve a high IIP3, the employment of negative feedback circuits and the increase of collector currents are a widely used

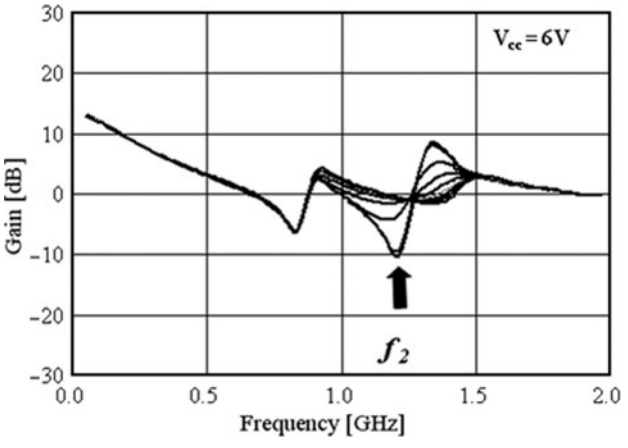

Fig. 16. Measured gain for a varied value of V_{c4} and a fixed value of V_{c3}.

https://doi.org/10.1017/S1759078709990390 Published online by Cambridge University Press

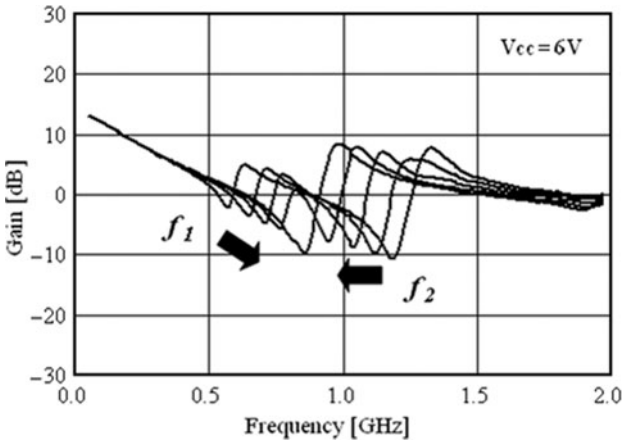

Fig. 17. Variation of the number of stopband with the control of V_{c1} and V_{c2}.

approach. A schematic diagram of the lossy match and negative feedback configurations is shown in Fig. 20. Two-tone characteristics are measured for the negative feedback circuit in Fig. 20 (b) with a parameter of the feedback resistance (R_F). Two tones of $f_1 = 1.08$ GHz and $f_2 = 1.1$ GHz were chosen. The measured gain and IIP_3 with a parameter of R_F are shown in Fig. 21. The measurement was done on the condition that $V_{cc} = V_{c1} = V_{c2} = 6$ V and $V_{c3} = V_{c4} = 6.6$ V.

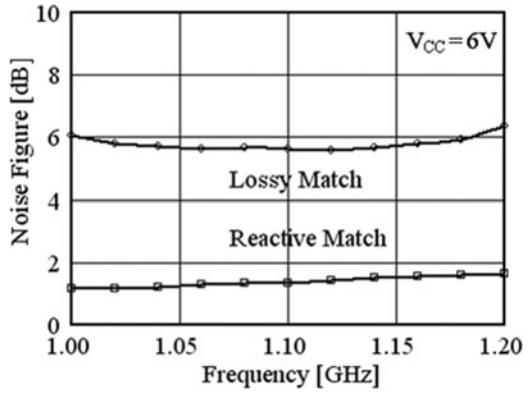

Fig. 18. Measured noise figure performance of the lossy match and reactive match amplifiers.

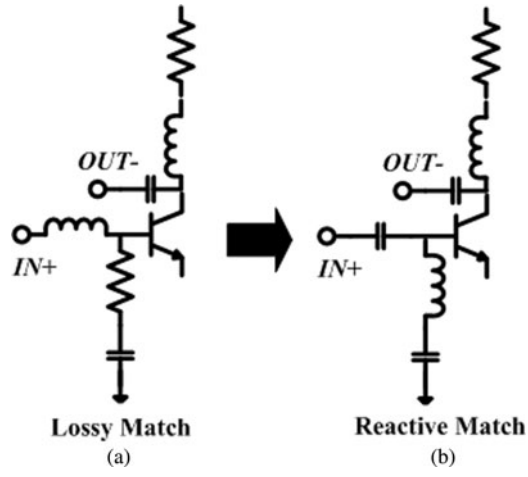

Fig. 19. Schematic diagram of the lossy match and reactive match configurations.

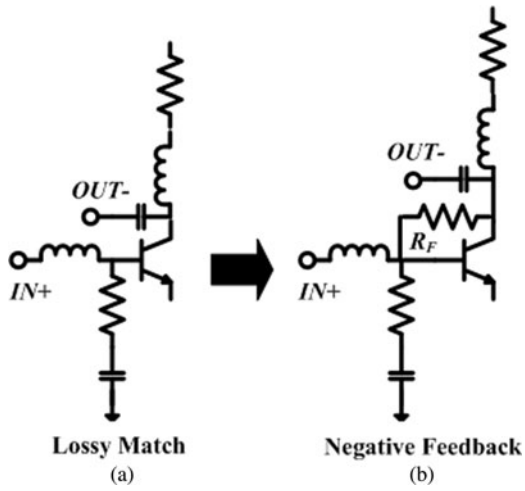

Fig. 20. Schematic diagram of the lossy match and negative feedback configurations.

As the feedback amount increases, that is, the value of R_F becomes small, the gain drops steeply but IIP_3 significantly improves. Two-tone characteristics are also measured for the lossy match circuit in Fig. 20 (a). The measured P_{1dB} is +3 dBm and IIP_3 is 0 dBm with $V_{cc} = 6$ V and $I_c = 8$ mA, which corresponds to an infinity of R_F in Fig. 21.

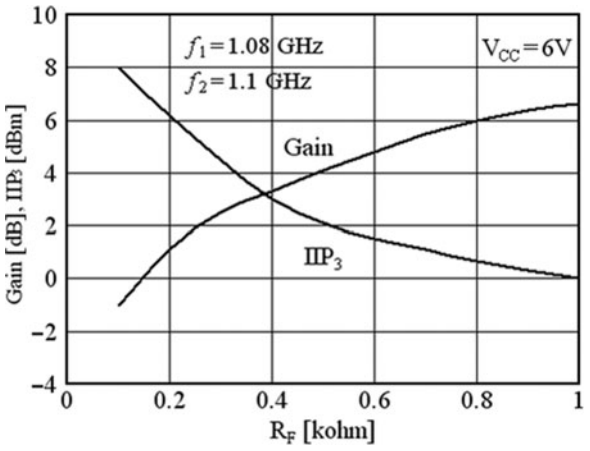

Fig. 21. Measured gain and IIP_3 with a parameter of R_F for the negative feedback configuration.

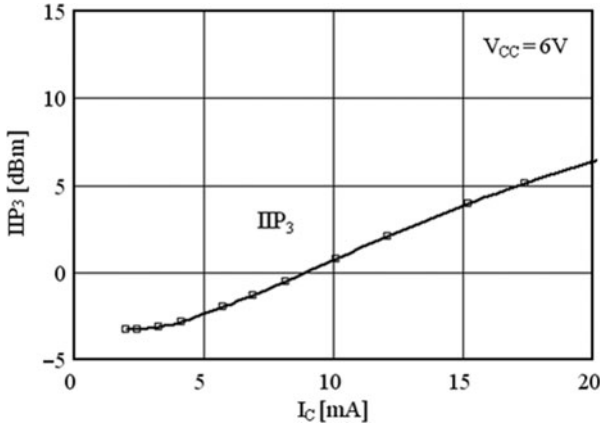

Fig. 22. Measured IIP_3 with a parameter of I_C.

https://doi.org/10.1017/S1759078709990390 Published online by Cambridge University Press

The other approach to improve IIP_3 is to increase collector current (I_C). The measured IIP_3 with a parameter of I_C is shown in Fig. 22. As I_C increases from 8 to 20 mA, an improvement of IIP_3 up to 6.5 dB has been achieved. This approach provides a compromise between IIP_3, power consumption, and noise figure performance.

V. CONCLUSIONS

The L-band frequency and rejection-level tunable SiGe HBT differential amplifier with dual stopband has been presented. In order to achieve frequency and rejection-level tunable performance, dual LCR-tank circuit with an active load was incorporated into the design of the series feedback loops of the differential amplifier. The implemented 0.35 mm SiGe HBT amplifier with dual stopband shows a frequency tuning of 0.53–1.16 GHz and a rejection-level variation up to 9.5 dB. The input and output return losses are better than 17.5 and 11 dB over 0.2–1.5 GHz, respectively. The measured P_{1dB} is +3 dBm and IIP_3 is 0 dBm with $V_{cc} = 6$ V and $I_c = 8$ mA. The data shown in the paper are limited to a 1 GHz band. For future WLAN applications, the operating frequency is due to be increased up to 2 and 5 GHz bands. The results obtained in the paper demonstrate that the frequency and rejection-level tunable differential amplifier with multiple stopband would be one of the candidates as an active interference canceller for the next-generation, adaptive and/or reconfigurable wireless radios.

REFERENCES

[1] McCune, E.: High-efficiency, multi-mode, multi-band terminal power amplifiers. IEEE Microwave Mag., **3** (2005), 44–55.

[2] Banbury, D.; Fayyaz, N.; Safavi-Naeini, S.; Nikneshan, S.: A CMOS 5.5/2.4 GHz Dual-band Smart-antenna Transceiver with a Novel RF dual-band phase shifter for WLAN 802.11a/b/g. IEEE Radio Frequency Integr. Circuit Symp. Dig. (2004), 157–160.

[3] Hossein, S.; Lavasani, M.; Chaudhuri, B.; Kiaei, S.: A pseudo-concurrent 0.18 μm multi-band CMOS LNA. IEEE MTT-S Dig. (2003), 181–184.

[4] Magnusson, H.; Olsson, H.: Multiband multi-standard transmitter using a compact power amplifier driver. IEEE Radio Frequency Integr. Circuit Symp. Dig. (2005), 491–494.

[5] Raghavan, A.; Gebara, E.; Tentzeris, M.; Laskar, J.: An active interference canceller for multistandard collocated radio. IEEE MTT-S Dig. (2005), 723–726.

[6] Chen, W.; Chang, S.; Huang, G.; Jean, Y.; Yeh, T.: A Ku-band interference-rejection CMOS low-noise amplifier using current-reused stacked common-gate topology. IEEE Microwave Wirel. Compon. Lett., **17** (2007), 718–720.

[7] Nguyen, T.; Oh, N.; Cha, C.; Oh, Y.; Ihm, G.; Lee, S.: Image-rejection CMOS low-noise amplifier design optimization techniques. IEEE Trans. Microwave Theory Tech., **53** (2005), 538–545.

[8] Zhang, S.; Madie, J.; Bretchko, P.; Makoro, J.; Shumovich, R.; McMorrow, R.: A novel power-amplifier module for quad-band wireless handset applications. IEEE Trans. Microwave Theory Tech., **51** (2003), 2203–2310.

[9] Hashemi, H.; Hajimiri, A.: Concurrent multiband low-noise amplifiers – theory, design, and applications. IEEE Trans. Microwave Theory Tech., **50** (2002), 288–301.

[10] Nakajima, H.; Muraguchi, M.: Dual-frequency matching technique and its application to an octave-band (30–60 GHz) MMIC amplifier. IEICE Trans. Electron., **E80-C** (1997), 1614–1621.

[11] Lin, Y.; Lu, S.: A 2.4/3.5/4.9/5.2/5.7-GHz concurrent multiband low noise amplifier using InGaP/GaAs HBT technology. IEEE Microwave Wirel. Compon. Lett., **14** (2004), 463–465.

[12] Itoh, Y.; Shinohara, T.; Shirata, M.; Sakamoto, K.: Eightfold-band differential SiGe HBT amplifier using stacked LC-tank circuits, in Proc. Asia-Pacific Microwave Conf., (2008), A1–47.

[13] Jachowski, D.: Compact, frequency-agile, absorptive bandstop filters. IEEE MTT-S Dig. (2005), 513–516.

[14] Itoh, Y.: L-band SiGe HBT differential amplifiers with multiple bandpass or bandstop performance using stacked parallel-resonant circuits. Contemp. Eng. Sci., **1** (2008), 127–138.

[15] Shirata, M.; Shinohara, T.; Sato, M.; Itoh, Y.: An L-band SiGe HBT differential amplifier with frequency-tunable and multiple stopbands. Proc. EuMA (2008), 151–154.

[16] Gray, P.; Hurst, P.; Lewis, S.; Meyer, R.: Analysis and Design of Analog Integrated Circuits, John Wiley & Sons, USA Inc., 2001.

Masaki Shirata received the B.E. degree in electrical and electronic engineering from Shonan Institute of Technology in 2008. He is now a student of the master course of electrical and information engineering in Shonan Institute of Technology. His research interest is in microwave low-noise amplifiers for multi-band and multi-mode applications. He is currently a student member of IEICE Japan.

Toshio Shinohara received the B.E. and M.S. degrees in electrical and electronic engineering from Shonan Institute of Technology in 2007 and 2009, respectively. He joined the Miharu Communications Inc. in 2009 and is now working on the research and development of CATV and optical communication systems. He is currently a member of IEICE Japan.

Minoru Sato received the B.E. degree in electrical and electronic engineering from Shonan Institute of Technology in 2008. He joined the Chiyoda Keiso Co. Ltd. in 2008. He is working on the research and development of new clean energy systems, global environment-friendly technologies, etc. based on a wide range of constituent engineering technologies, which have been applied in various types of plants for the past several years.

https://doi.org/10.1017/S1759078709990390 Published online by Cambridge University Press

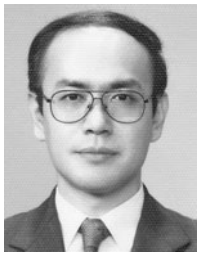

Yasushi Itoh received the B.S., M.S., and D.E. degrees in electronic engineering from Waseda University, Tokyo, Japan, in 1978, 1981, and 1989, respectively. He joined Tokimec Inc. in 1981, where he has worked on the R&D of broadband low-noise amplifiers and oscillators. In 1990, he joined Mitsubishi Electric Corporation, Information Technology R&D Center, where he has been engaged in the research and development of microwave and millimeter-wave low-noise and high-power MMIC amplifiers and solid-state power amplifiers. From 2000 to 2003, he has been a visiting professor of the Cooperative Research Center of the University of Electro-Communications, Tokyo, Japan. In 2003, he joined the Shonan Institute of Technology, Kanagawa, Japan, as a professor of the Department of Electrical & Electronic Media Engineering. In 2000, he received the Electronics Society Award from IEICE Japan. He is s Senior Member of the IEEE.

https://doi.org/10.1017/S1759078709990390 Published online by Cambridge University Press